Electronic structure of self-organized InAs/GaAs quantum dots bounded by {136} facets

Weidong Yang, Hao Lee, Thomas J. Johnson, and Peter C. Sercel
Department of Physics, University of Oregon, Eugene, Oregon 97403

A. G. Norman
National Renewable Energy Laboratory, Golden, Colorado 80401

(Received 29 July 1999)

Recent experiments indicate that the shape of self-organized InAs quantum dots grown on GaAs [001] is an elongated pyramid with bounding facets corresponding to a family of four {136} planes. This structure, which possesses C_{2v} symmetry, is quite different from square-base pyramidal or lens geometries, which have been assumed in previous electronic structure calculations for this system. In this paper, we consider theoretically the influence of the {136} shape on the electronic structure and optical properties of the quantum dots. We present a valence force-field calculation of the inhomogeneous strain and incorporate the results into an eight band $\vec{k}\cdot\vec{p}$ electronic structure calculation. The size dependence of the electronic structure is calculated and compared to experimental photoluminescence spectra. The effects of perturbations on the {136} shape are also considered. Calculations based on the {136} shape give good agreement with the observed level structure and optical polarization properties of self-organized InAs/GaAs quantum dots.

I. INTRODUCTION

The demonstration that defect-free quantum dot (QD) structures may be fabricated directly by utilizing the coherent island Stranski Krastonov growth mode[1,2] has spurred tremendous experimental and theoretical research effort in recent years directed at understanding the electronic and optical properties of these structures. Many features of the electronic and optical properties of InAs/GaAs QD's grown by this technique have been revealed in recent experiments. The quasi-atomic character of the joint density of states for optical transitions has been demonstrated.[3,5] Furthermore, photoluminescence spectra at high excitation intensity exhibit a well-resolved excited state structure,[6,7] which is consistent with the results of resonant photoluminescence and photoluminescence excitation measurements.[8–10] Complementary experiments using capacitance methods reveal a similar general picture of the carrier density of states in these structures.[11,12] The high quality of the available samples coupled with the richness of the spectroscopic data thus far reported has motivated a number of calculations of the electronic structure of InAs/GaAs QD's. While calculations have been performed to varying levels of approximation, all such studies necessarily contain assumptions regarding the QD shape.

A number of experimental studies have been reported, which attempt to address the question of the shape of InAs/GaAs self-organized QD's. Atomic force microscope (AFM) images of self-organized dots appear to show a lenslike morphology[13,14] which motivated electronic structure calculations assuming cone[16] or len shapes[17] for the dots. However, AFM is not capable of resolving the detailed shape of InAs/GaAs QD's due to the tip-convolution effect. Likewise, transmission electron microscopy (TEM) performed under the usual dynamical two-beam imaging conditions images the strain field within the structure and in the surrounding material and is consequently incapable of resolving the QD shape.[1,4,15] In an attempt to circumvent this problem, Ruvimov *et al.* reported [001] on-zone bright-field images of self-organized InAs/GaAs QD's in plan view. The images of the dots appear square shaped with edges aligned close to the $\langle 100\rangle$ directions.[18] In conjunction with cross-sectional imaging it was concluded that the QD's possessed a square-based pyramidal geometry with bounding planes near {101}. Naturally, this morphology has served as the basis of several electronic structure calculations.[19–22] However, multiple-beam dynamical image simulations recently performed by Liao *et al.* demonstrate that even a spherical InAs QD can produce square-shaped images under the imaging conditions employed by Ruvimov *et al.* – the symmetry of these images is determined primarily by the underlying *lattice* rather than the overall shape of the QD.[23] This result undermines the basis for the hypothesis that the self-organized QD's grown by molecular-beam epitaxy (MBE) possess a square-based pyramidal shape.

Recently, experimental results have been reported, which suggest that the shape of self-organized InAs QD's grown by MBE on (001) GaAs is not a square-based pyramid but rather an elongated facetted structure bounded by {136} planes.[24–27] The {136} structure possesses a parallelogram base and C_{2v} symmetry, quite different from lens or square-base pyramidal geometries that have been assumed in electronic structure calculations. These experimental results, based on reflection high-energy electron diffraction (RHEED),[24,25] TEM,[26] and AFM,[27] are breifly summarized in Sec. II, below.

The purpose of the present paper is to address the question: If the shape of self-organized InAs/GaAs QD's after capping with GaAs is correctly described by the {136} facet model, what influence does this shape have on the electronic structure and optical properties of the QD's? To answer this question we describe in Sec. III an atomistic valence force-field calculation of the inhomogeneous strain tensor of InAs/GaAs QD's possessing the {136} structure. These results are

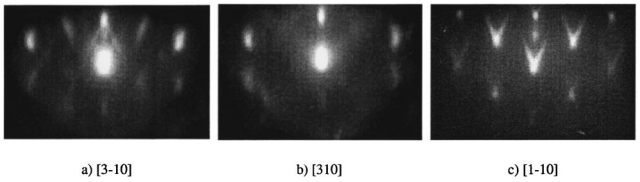

FIG. 1. RHEED patterns of self-organized InAs QD's along (a), $[3\bar{1}0]$, (b), [310], and (c), $[1\bar{1}0]$ azimuths after deposition of 1.68 monolayers of InAs. The included angle of the chevrons in (c) is 50° while the streaks in panel (a), which are believed to be facet-related, have a separation angle of 56°.

input into an eight band $\vec{k}\cdot\vec{p}$ electronic structure calculation. The dependence of the electronic structure on size is investigated and the results are compared with experimental photoluminescence results in Sec. IV. To further test the model, in Sec. V, we present polarization-resolved photoluminescence (PL) spectra that exhibit multiple excited state transitions, each of which shows strong in-plane polarization anisotropy. We show that, while this experimental observation is inconsistent with previous electronic structure models of InAs/GaAs QD's, the in-plane optical polarization anisotropy can be understood quantitatively by consideration of the asymmetric shape of the QD structures. Also in this section, the effect of perturbations to the {136} shape on the electronic structure and optical spectra is considered computationally. The main conclusion of this discussion is that polarization measurements provide a more stringent test of electronic structure models than simple comparison to PL peak positions; polarization anisotropy provides a signature that is uniquely sensitive to the QD symmetry.

II. THE {136} FACET MODEL FOR THE QUANTUM DOT SHAPE

As stated in the introduction, interpretation of TEM and AFM images of self-organized InAs/GaAs QD's has been problematic owing to the small size and high degree of strain in these structures. The consequent uncertainty regarding the shape has been a key obstacle in establishing structure/property relationships for this system. For this reason, the determination of the precise shape of self-organized InAs/GaAs QD's has been a problem of the utmost importance.

Recent experiments have provided data that significantly constrain models for the shape of self-organized InAs/GaAs QD's.[24,26] The first of these, by Lee *et al.* consisted of a measurement of the RHEED patterns as a function of the azimuthal angle. Figure 1 shows the RHEED patterns observed along the $[3\bar{1}0]$, [310], and $[1\bar{1}0]$, azimuths. The upward-directed chevrons observed along the $[1\bar{1}0]$ azimuth (panel(c)), with an included angle of 50° were previously interpreted as originating from {113} bounding facets Refs. 28 and 29. However, RHEED patterns measured along the $[3\bar{1}0]$ and $[1\bar{3}0]$ azimuths show facet-related *streaks*, which had not been previously observed and which are not consistent with this interpretation. The pattern along $[3\bar{1}0]$ is shown in Fig. 1(a); the pattern along $[1\bar{3}0]$ was found to be identical. The facet-related streaks seen along these azimuths are directed at an angle of 28° from the [001] direction. No

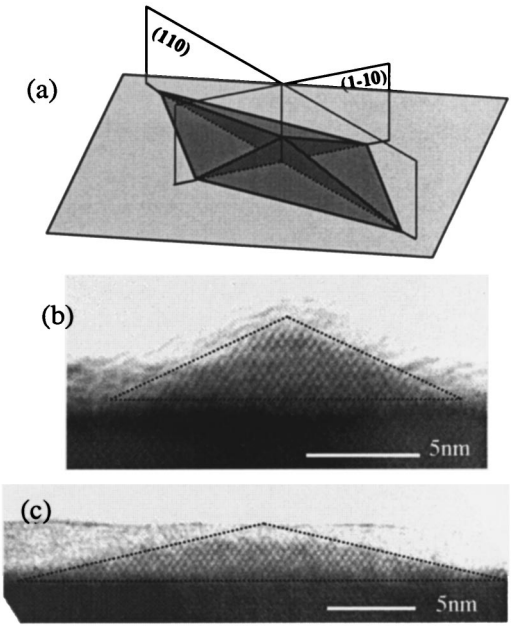

FIG. 2. InAs QD bounded by {136} facet planes. (a): 3D model showing sections contained in the (110) and (1-10) planes. (b,c): Cross-sectional HRTEM images of uncapped InAs QD's sectioned in the (1-10) and (110) planes, respectively. The dashed lines inside these images are superimposed profiles corresponding to the ideal {136} structure.

streaks were observed at any other azimuth, including the [130] and [310] directions as shown in panel (b). These observations, as well as the upwards-pointing chevrons observed along the $[1\bar{1}0]$ azimuth, are consistent with bounding facets of the {136} family.[24,26] The {136} pyramidal structure inferred from these experiments is depicted in Fig. 2. The structure possesses a parallelogram base with a 2:1 in-plane elongation along [1-10]; the length:width:height ratio of the inferred structure is $2:1:\sqrt{2}/6$. This shape anisotropy was also directly supported by cross-sectional high resolution transmission electron micrographs (HRTEM) of uncapped InAs island samples grown on GaAs and sectioned along the $[1\bar{1}0]$ and [110] axes, as shown in panels (b) and (c) of Fig. 2. The width-to-height ratios in Figs. 2(b) and 2(c), which are representative of several micrographs, closely match the {136} facet structure as the overlaid model cross-sectional profiles show: The height to width is close to 1:4 in the $(1\bar{1}0)$ section and to 1:8 in the (110) plane. The dashed lines inside these images represent the superimposed side-view shapes from Fig. 2(a). They show that the shape of the InAs QD's matches well with the {136} model along the [110] and $[1\bar{1}0]$ directions. These results were confirmed by Saito *et al.* who reproduced the RHEED patterns corresponding to {136} facets in InAs/GaAs self-organized dots, and by Yoon *et al.* who were able to directly image by AFM, the {136}-bounding facets of InAs QD's grown on InGaAs lattice matched to InP.[27] Direct AFM imaging of the QD shape in Yoon's experiment was made possible by the fact that the $InAs/In_xGa_{1-x}As$ coherent islands are four to five times larger than in the InAs/GaAs system by virtue of the smaller lattice mismatch, significantly ameliorating the tip-convolution problem.

It should be emphasized that the {136} model proposed by Lee *et al.* is based upon measurements performed on InAs islands prior to their being capped with GaAs. The capping step is necessary for photoluminescence studies, and unfortunately its effect on the structure of the dots is difficult to characterize. In the next section we take up the problem of determining the electronic structure of InAs self-organized QD's under the *assumption* that the structures retain a sharp upper interface between the InAs dot and the GaAs barrier which is defined by {136} planes even after capping. In Sec. V, we return to the question of possible structure changes during capping by considering the effect of variations to the {136} facet structure such as truncation or rounding of the dot/barrier interface.

III. CALCULATION OF THE STRAIN AND ELECTRONIC STRUCTURE

A. Valence force-field calculation of the strain

Due to the large lattice mismatch ($\approx 7\%$), the starting point of any calculation of the electronic structure of self-organized InAs/GaAs is necessarily a determination of the strain distribution within the structure since this will modulate the band edge energies through the action of the deformation potentials.[30] We use the atomistic valence force-field (VFF) model developed by Keating[31,32] to calculate the strain distribution, an approach that has recently been employed by several others to determine the strain distribution in InAs/GaAs QD's of square-based pyramidal shape.[20,21] This model has been shown to be successful in fitting and predicting the elastic constants of elastic continuum theory. It has been successfully applied to the calculation of strain distribution in quantum wells and the atomic structure of semiconductor alloys.[33–35] Due to the small size and shallow geometry of the QD's in this study (less than 4 nm height), the VFF model has the advantage over elastic continuum theory of avoiding potential failure in the atomically thin limit. In the VFF model, the total energy of a lattice is expressed as

$$V=\frac{1}{4}\sum_{ij}\frac{3}{4}\alpha_j(d_{ij}^2-d_{0,ij}^2)^2/d_{0,ij}^2 + \frac{1}{2}\sum_{i}\sum_{j\neq k}\frac{3}{4}\beta_{ijk}(\vec{d}_{ij}\cdot\vec{d}_{ik}+d_{0,ij}d_{0,ik}/3)^2/d_{0,ij}d_{0,ik}. \quad (1)$$

Here, the α and β terms respectively describe the contributions of bond stretching and bond bending to the total energy. We take the bond-stretching and bending parameters developed for InAs and GaAs by Martin.[32] The geometric average of the bond-bending parameters of InAs and GaAs is used for the atomic configuration In-As-Ga. Using periodic boundary conditions, a supercell of 10^6 atoms containing an InAs QD of a particular structure is constructed with initial atom placements corresponding to that of bulk GaAs. Starting from this initial lattice configuration, the lattice is relaxed to the global energy minimum using the conjugate gradient method. Local strain tensors ($\tilde{\epsilon}$) are then calculated at each cation site by studing the deformation of a tetrahedron formed by four nearest-neighboring anions.[36] The strain tensor for each unit cell is taken as the average of the tensors for the four cation sites within the cell.

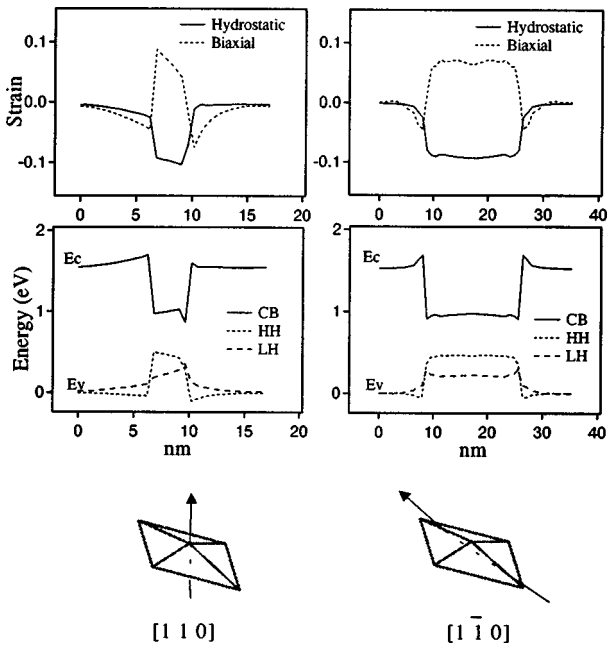

FIG. 3. Strain and band edge profiles in an InAs QD bounded by {136} planes embedded in GaAs. Top: Calculated hydrostatic and biaxial components of strain for a dot of 29 nm length plotted along the [001] direction through the center of the dot (top left) and along $[1\bar{1}0]$ at the half height position (top right). Bottom: Band edges modified by the local value of the strain plotted along the same lines as in the top panels.

The resulting strain distribution for a 29 nm long QD with {136} bounding facets structure is depicted in Fig. 3. The hydrostatic and biaxial components of strain, respectively denoted ϵ_h and ϵ_b, are plotted along special symmetry lines, which are shown in the model in Fig. 3(a). Here $\epsilon_h = Tr\tilde{\epsilon}$ and $\epsilon_b = 2\epsilon_{zz}-\epsilon_{xx}-\epsilon_{yy}$.[20] As noted in Ref. 20, the strain is primarily compressive in the QD and tensile in the GaAs barrier, with a significant compressive biaxial component in the QD. Figure 3(b) shows the band edges modified by the local value of the strain, calculated using the deformation potentials of Van der Walle.[37] A key parameter used in calculation of the band structure is the unstrained valence-band offset E_{vbo} between InAs and GaAs. We use 85 meV following Pryor,[22] which was determined by analysis of transition-metal impurity spectra in the respective bulk semiconductor materials. A summary of all numerical parameters used in the calculations appears in Table I.

B. Eight-band $\vec{k}\cdot\vec{p}$ calculation of electronic structure

To calculate the electronic structure of the {136}-bounded InAs/GaAs QD, we employ an eight-band envelope function formalism. The technique consists of solving the eigenvalue equation,

$$\sum_j \{H_{i,j}(-i\hbar\nabla,\vec{r})+H_{\mathrm{Str}}[\tilde{\epsilon}(\vec{r})]\}F_j(\vec{r})=EF_i(\vec{r}). \quad (2)$$

Here the operator $H_{i,j}(-i\hbar\nabla,\vec{r})$ is derived from the eight-band $\vec{k}\cdot\vec{p}$ Hamiltonian describing coupling among the

TABLE I. Parameters

VFF Parameters	InAs	GaAs
a(Å)	6.0583	5.65325[b]
$\alpha(N/m)$	35.18	41.19[a]
$\beta(N/m)$	5.50	8.95[a]
k·p Parameters	InAs	GaAs
γ_1	19.7	6.85[b]
γ_2	8.4	2.10[b]
γ_3	9.29	2.90[b]
E_g(eV)	0.418	1.5192[b]
δ(eV)	0.38	0.341[b]
E_p(eV)	20.2	22.71[b]
E_{vbo}(meV)	85 [d]	–
Deformation Potentials	InAs	GaAs
a_c(eV)	-5.08	−7.17[c]
a_v(eV)	1.00	1.16 [c]
b(eV)	-1.8	−1.6[c]
d(eV)	-3.1	−4.23[c]

[a]R. M. Martin (Ref. 32).
[b]Landolt-Börnstein (Ref. 42) and Jiang (Ref. 21).
[c]Van der Walle (Refs. 37).
[d]Craig Pryor (Ref. 22).

two conduction and six valence bands, by the replacement $\vec{k} \rightarrow -i\hbar\nabla$, and by taking the band-edge energies and mass parameters to be functions of position. The eight-band $\vec{k}\cdot\vec{p}$ Hamiltonian is an extension of the Luttinger-Kohn (LK) formalism,[38,39] which describes coupling among the Γ_8 and Γ_7 valence band states to second order in $\vec{k}$ but is modified to include explicitly the linear $\vec{k}\cdot\vec{p}$ coupling between the conduction and valence band states.[40,41] The importance of using an eight band model to describe the electronic structure of InAs/GaAs self-organized QD's, and the errors incurred by using a single band discription of the electron states and either a single-band, four-band or six-band description of the hole states, have been described in detail in a careful study by Pryor.[22] In Eq. (2) the operator $H_{Str}(\tilde{\epsilon}(\vec{r}))$ describes the effect of the inhomogeneous strain $\tilde{\epsilon}(\vec{r})$ on the electronic structure. The valence band deformation potential terms are found in Refs. 30 and 41. In our calculations we neglect the lack of inversion symmetry in the zincblende structure and consequently neglect the shear deformation potential for the conduction band. We also neglect the strain interactions originating from spin-orbit coupling since they are small.[41] In this paper we also neglect the piezoelectric potential. We found that piezoelectric potential is generally less than 30 meV for the dot sizes studied and the resulting effect on the level positions is on the order of 1 meV.

The eigenvalue problem represented by Eq. (2) was solved numerically using finite-difference methods. The grid spacing is chosen to be the GaAs lattice constant in all three directions. In order to get correct boundary counditions and maintain the Hermiticity of the Hamiltonian, first and second order derivatives on the boundary are chosen according to the symmetrization scheme[43]

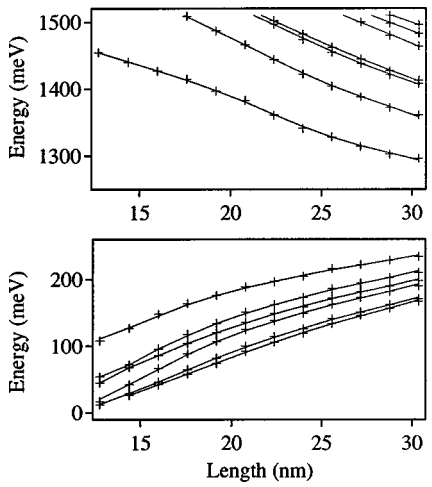

FIG. 4. Calculated electronic structure of InAs/GaAs QD's versus QD length. Top: electron states. Bottom: hole states.

$$\gamma\hat{k}_i\hat{k}_j \rightarrow (\hat{k}_i\gamma\hat{k}_j + \hat{k}_j\gamma\hat{k}_i)/2$$

$$P\hat{k}_i \rightarrow (P\hat{k}_i + \hat{k}_iP)/2,$$

where γ in the first expression denotes a Luttinger parameter and P in the second denotes the Kane matrix element. In the finite-difference scheme, the Hamiltonian is transformed into large sparse matrices of size up to 10^6. Eigenvalues of interest are then solved using PARPACK, an implementation of the implicitly restarted Arnoldi-Lanczos methods.[44] Computation was done on a Silicon Graphics Power Onyx with eight R10000 CPUs at Computational Science Institute at University of Oregon. In our calculations, we have used the electronic structure parameters for InAs and GaAs which are tabulated in Landolt-Börnstein,[42] indentical with those employed by Jiang and Singh in their eight-band calculations of InAs/GaAs QD's of square-base pyramidal geometries.[21]

IV. CALCULATED ELECTRONIC STRUCTURE AND COMPARISON TO EXPERIMENT

Using the techniques described in the last section we have calculated the electronic structure of InAs/GaAs QD's with the {136} QD structure as a function of the dot size. The results are depicted in Fig. 4, which shows the energies of all bound electron and hole states as a function of QD length. The zero of energy is taken to be the bulk GaAs valence-band edge. Figure 5 shows isosurface plots of the dominant envelope function components, F [see Eq. (2)], of the first several electron and hole wave functions. As apparent in this figure, the envelope functions of both the ground electron and hole states have predominantly *s*-like character and the first two excited states of the electrons and the holes have predominately *p*-like character. It should be emphasized that, while the total probability density for each state does not posses nodal planes as pointed out by Wang *et al.*,[45] the different components of the wavefunction associated with different Bloch functions do possess nodal planes as a consequence of the the mirror plane symmetries of the dot structure. Due to the C_{2v} symmetry of the Hamiltonian, each energy eigenstate has only the two-fold degeneracy associated with time-reversal symmetry.

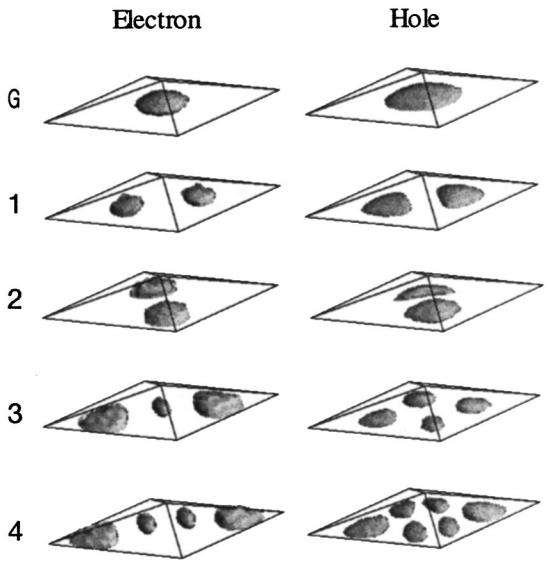

FIG. 5. Isosurface plots of the dominant envelope function components of the five lowest energy electron and hole states of a {136} InAs QD embedded in GaAs. The length of the dot is 27 nm. The lowest energy states are labeled *G* while the excited states are numbered in the order of increasing energy.

In the {136} structure the first two electron *p* states are separated by about 45 meV over a wide range of sizes, while the first two hole *p* states are separated by about 15 meV. These large separations are due to the 2:1 length:width ratio of the {136} structure. For comparison, the separations of the corresponding states in square pyramidal dots bounded by {101} planes are below 10 meV according to our calculations. The small *p*-state splitting we find in square-based dots is due to strain asymmetry. Although a pyramidal *shape* has a four-fold rotation symmetry, the underlying tetrahedral lattice does not. Consequently, the Hamiltonian of a square pyramidal dot has C_{2v} symmetry due to the atomic level asymmetry, which enters into our atomistic calculation of the strain.

A somewhat counter-intuitive feature of the results shown in Fig. 4 is that the electron and hole eigenenergies decrease approximately linearly with increasing QD size so that the subband separations for electron or hole states are relatively insensitive to QD size. This effect is clearly at variance with the $1/r^2$ scaling expected in simple particle-in-a-box quantum confinement models and is due to competition between the size dependence of the dot strain and quantum confinement effects. As a result, intraband transitions in self-organized dots should be far less sensitive to inhomogeneous broadening than interband transitions, a feature which is potentially useful in the design of devices such as QD infrared photodetectors.

To test the level structure calculated for the {136} QD structure, we present in Fig. 6 a comparison of experimental PL spectra and calculated polarization-averaged transition dipoles for {136} QD's. Figure 6(a) shows experimental low temperature PL spectra taken of an ensemble of QD's as a function of pump power. The sample used in these measurements was grown at 530 °C and capped with 50 nm of GaAs at the same temperature. The relatively high growth temperature was chosen because we have found that under these

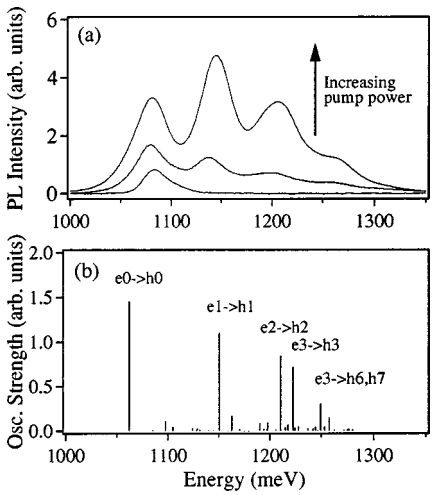

FIG. 6. Comparison of calculated and experimental optical spectra. Panel (a): Experimental PL spectra for various pump powers. Panel (b): Calculated oscillator strength of {136}-shaped QD of length 27 nm.

conditions the dots exhibit multiple excited-state transitions and relatively narrow linewidths. PL spectra were obtained under excitation with the 488-nm line of an Ar-ion laser, taken at a sample temperature of 10 K in a closed cycle He cryostat and detected with a liquid nitrogen cooled Ge pin detector using standard lock-in detection methods. Due to the state-filling effect, a number of resolvable excited state transitions emerge in the sample with increasing excitation level. The average length of QD's in samples identically grown but not capped with GaAs was determined by AFM to be approximately 30 nm. In Fig. 6(b), we present the calculated polarization-averaged squared optical transition-matrix elements and transition energies of the lowest several interband transitions in a QD structure bounded by {136} facets and with length 27 nm. This length was chosen to reproduce the experimental ground-state transition energy.

A key prediction of the model shown in Fig. 6(b) is that the third major transition observed should consist of a doublet involving the $e_2 \rightarrow h_2$ and $e_3 \rightarrow h_3$ transitions. In practice, these two transitions lie too close together in energy to be resolved in an ensemble PL spectrum due to size-related inhomogenous line broadening. However, the existence of a doublet transition should be manifested by an enhanced apparent linewidth. Indeed, inspection of the experimental PL spectra [Fig. 6(a)] shows that the third peak in the measured spectra has a significantly larger full width at half maximum (FWHM) than the first two peaks. The enhanced linewidth of the third peak has previously been noted by other investigators but was attributed to energy dependence of the inhomogeneous linewidth.[7] Specifically, the excess linewidth was explained in terms of the increased sensitivity to size broadening of higher energy states which is expected in simple particle-in-a-box models.[7] However, as discussed above, in self-organized dots the electron and hole energies decrease approximately linearly with increasing QD size, so that the inhomogeneous linewidth should be roughly independent of transition energy. The fact that the third peak has a larger FWHM relative to the two lower energy transitions therefore supports the assignment of this peak to the doublet $e_2 \rightarrow h_2$ and $e_3 \rightarrow h_3$ transitions. In the next section, we present

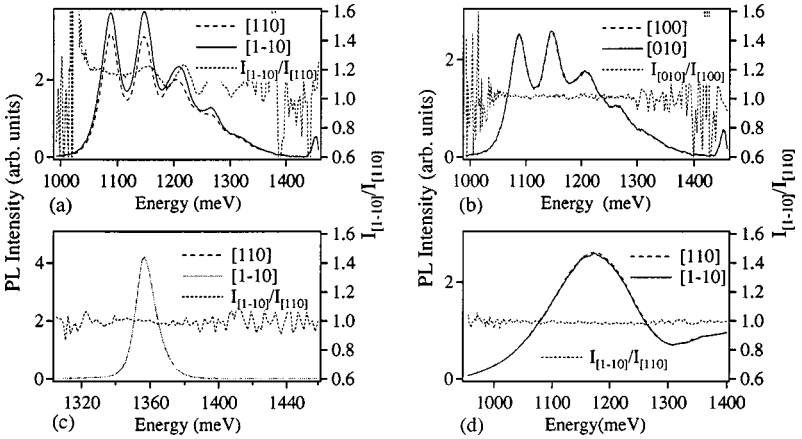

FIG. 7. Polarization-resolved PL spectra. (a): InAs/GaAs QD's measured with polarizer set along [110] and [1-10] axes; (b): InAs/GaAs QD's measured with polarizer set along [100] and [010] axes; (c) and (d): PL of $In_xGa_{1-x}As$ quantum well and $N+$ GaAs substrate, respectively, with polarizer set along the [110] and [1-10] axes. In all spectra the ratio of the PL intensity along the two orthogonal polarization directions is plotted against the right hand axis of the graph.

polarization-resolved PL data which confirm this assignment.

Referring to Fig. 4, we also note that the model predicts that self-organized InAs/GaAs QD's with ground-state transition energy greater than 1.3 eV possess only a single-bound electron state. Since the optical transition-matrix elements are negligible for transitions labeled $e_0 \rightarrow h_i$, for number $i > 0$, such small QD's are predicted to exhibit only a single major PL transition in ensemble measurements, as observed experimentally by many groups including our own. This result has important implications to the interpretation of nonlinear PL spectra of single QD's, which will be explored in a future paper.

It should be noted that other electronic structure calculations that have assumed highly symmetrical shapes, including cones, lenses, and square-based pyramids, have been used previously to interpret the PL spectra of self-organized InAs/GaAs QD's. Further approximations made in previous studies have included the neglect of valence-band-coupling effects,[19] neglect of conduction/valence-band coupling,[20] and the neglect of spin-orbit coupling.[46] Due to uncertainty in the detailed level structure owing to inhomogeneous broadening effects and the small number of resolvable excited state transitions (typically 1-4) it is difficult to distinguish with confidence among the various models on the basis of simple fits to spectral peak positions such as in Fig. 6. However, the geometrical asymmetry of the {136} structure clearly distinguishes it from previous models and should cause a polarization anisotropy in the plane of the dots, permitting a clear experimental test. We turn in the next section to a discussion of polarization-resolved PL measurements and a comparison of these results with the theory.

V. OPTICAL POLARIZATION ANISOTROPY

Polarization-resolved PL measurements were carried out using the same experimental apparatus as before but with the addition of a polarization analyzer between the sample and spectrometer. Pairs of polarization-resolved PL spectra were measured along orthogonal polarization axes by orienting a polarizing beam splitter cube at 45° and 135° from the groove direction of the grating. This way, grating-induced polarization artefacts are eliminated and the two orthogonal PL polarizations can be directly compared. Samples were also rotated to confirm that the polarization anisotropy observed was correlated with sample orientation and not due to other effects such as optical anisotropy or birefringence in the light collection system or polarization memory from the pump-laser beam. Samples were mounted on a copper cold finger using rubber cement to minimize mounting strain.

In Fig. 7, we present polarization-resolved PL spectra of InAs/GaAs QD's as well as experimental control samples including an $In_xGa_{1-x}As$ quantum well and a degenerately doped n-type GaAs substrate. The QD spectra were obtained under high excitation conditions where several excited-state transitions are resolved due to the state-filling effect. The polarization axes in the spectra of the InAs QD's depicted in Fig. 7(a) coincide with the the [110] and [1-10] axes of the sample (the short and long axes of the {136} structure, respectively). The spectra obtained from QD sample are clearly polarized along the long axis of the QD structures [Fig. 7(a)], while the polarization anisotropy of the control samples are less than 2% as shown in Figs. 7(c) and 7(d). The polarization ratio (long axis: short axis) of the ground transition in this InAs QD sample is 1.2, and the excited state transitions are predominantly polarized along the long axis as well. No in-plane polarization anisotropy was observed between the [100] and [010] directions in any sample we examined, as shown for example in Fig. 7(b). It was also confirmed that the observed optical polarization anisotropy was independent of the polarization of the pump laser, which was varied using a half-wave Fresnel rhomb.

Figure 8 shows a comparison of the experimental polarization-resolved PL spectra with the polarization-dependent optical transition-matrix elements (OME's) calculated for the {136} structure. To facilitate discussion, major transitions in the experimental spectra, panel (a), are labeled $T_0, T_1, \ldots$ for the ground- and excited state transitions, while the calculated transitions in panel(b) are labeled according to the participating states (en or hn for electron and hole states, respectively). The ground transition, $e0 \rightarrow h0$, has a calculated polarization ratio $I_{[1\bar{1}0]}/I_{[110]} = 1.74$ (compared to the experimental value of 1.2 for transition $T0$); the next three strongly allowed transitions are each predominantly polarized along the long axis of the structure in agreement with the experiment. The calculated anisotropy is due to the shape of the {136} structure rather than strain asymmetry. To illustrate this, the squared OME for the ground transition in square-based InAs QD's, calculated by us using the eight-band $\vec{k} \cdot \vec{p}$ model with strain determined by the VFF method, is larger along [110] than $[1\bar{1}0]$ by 3% for QD's bounded by {101} planes and by 2% for structures bounded

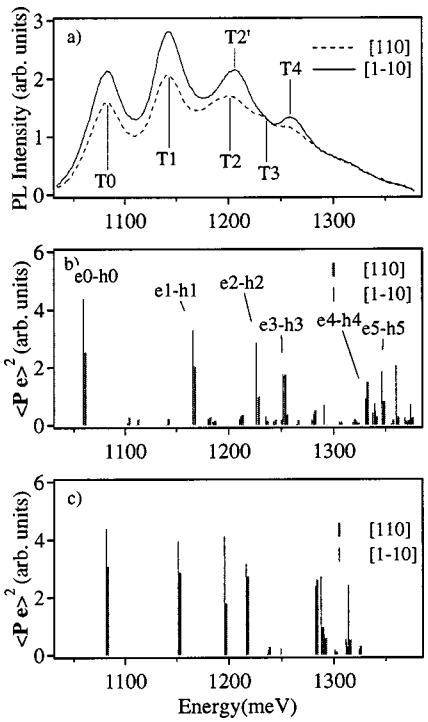

FIG. 8. Polarization-resolved PL spectra and comparison to theory. (a) Experimental PL with polarization axes along [110] and $[1\bar{1}0]$ directions (T = 15 K). (b): Squared OME's calculated for light polarized along [110] and $[1\bar{1}0]$ for the {136} structure (length 27 nm). (c): Same as panel(b) but for {136} structure terminated by a (001) plane cut at 50% height. The QD length has been increased to 33.5 nm to preserve ground transition energy.

by {105} planes. This is shown in Fig. 9. The breaking of the in-plane symmetry in these cases is due to the strain asymmetry between the [110] and $[1\bar{1}0]$ directions.[36] The effect of the strain-induced piezo-electric potential was also considered but was found to be small in comparison with the deformation potential effect.

A significant feature in the experimental spectra, Fig. 8(a), is the shift in the position of the second excited peak (labeled $T2$, $T2'$) with polarization and the reduction in linewidth with respect to the unpolarized spectra in Fig. 6(a). The linewidth narrowing and polarization shift can only be explained if this peak corresponds to an unresolved doublet: In the {136} model, the peaks $T2$, $T2'$ correspond to the doublet $e2 \rightarrow h2$, $e3 \rightarrow h3$ as discussed in the last section. While both transitions are strongest along $[1\bar{1}0]$, their relative strengths reverse with polarization, causing the shift in the PL spectra measured for [110] and $[1\bar{1}0]$ polarizations. Note, however, that the calculated shift has a direction opposite to that observed, indicating that the calculated order of the transitions is incorrect. The corresponding error of about 20 meV could be due to inaccuracy of the various material parameters used in the calculation, or to deviation of the true shape of the QD from the ideal {136} structure. For example, a narrowing of the QD along the short axis due to intermixing during capping can reverse the order of the second and third excited electron states and thus the direction of the polarization shift. Referring again to Fig. 8(a), the shoulder labeled $T3$, which is obscured in the unpolarized spectra, most likely corresponds to the weak unpolarized transition $e3 \rightarrow h6$. Finally, the calculated transitions $e4 \rightarrow h4$ and $e5 \rightarrow h5$, together with a large number of overlapping minor transitions, correspond roughly to peak $T4$.

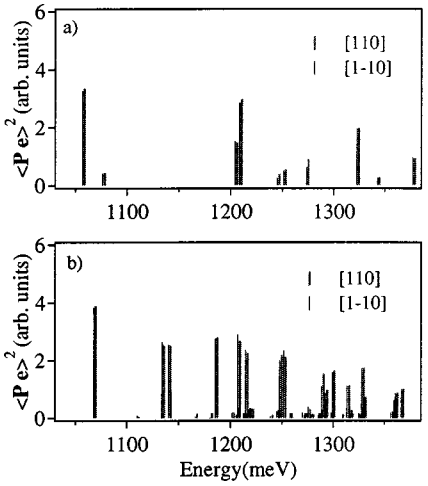

FIG. 9. Polarization-dependent optical matrix elements calculated for square-base pyramids bounded by {101} facets (a), and {105} facets (b). The base length of the pyramids was 11.3 and 26 nm in (a) and (b), respectively.

An important discrepancy between the experiment and the calculation for the {136} structure is that the peak spacings and polarization anisotropies calculated are systematically larger than observed [compare panels (a) and (b) in Fig. 8]. A likely explanation is that the QD shape changes during the capping step.[47] For instance, it has been reported that capped self-organized InAs/GaAs QD's possess flat top boundaries.[48] To model such an effect, we computationally investigated the effect of truncating the {136} structure by a (001) top plane. The magnitude of the polarization anisotropy and the splittings between the ground- and excited-state PL transitions were found to decrease with increasing degree of truncation. For example, truncation of the {136} structure at a position 50% from the top (15% volume reduction) reduces the calculated ground state polarization anisotropy to $I_{[1\bar{1}0]}/I_{[110]} = 1.42$ and brings the excited-state peak positions for the lowest three transitions into better agreement with the experiment [Fig. 8(c)].

As a preliminary experimental check that shape changes or intermixing during capping might explain why the polarization anistropy is smaller than calculated, we studied an InAs QD sample grown at a lower temperature of 500 °C and capped initially at 450 °C, so that intermixing effects should be relatively supressed. Although the excited-state transitions are not resolvable in this sample, the ground PL transition has a polarization ratio $I_{[1\bar{1}0]}/I_{[110]} = 1.4$, significantly larger than the sample grown and capped at higher temperature where intermixing should be more important. The polarization-resolved PL spectra of this sample are shown in Fig. 10. The larger anisotropy seen in the 500 °C sample could also be due to the smaller average dot size resulting from the lower growth temperature.[50] Our calculations show that the polarization anisotropy should increase with decreasing dot size as shown in Fig. 11. Indeed, the ground PL transition in Fig. 10 occurs at 1170 meV indicating that the

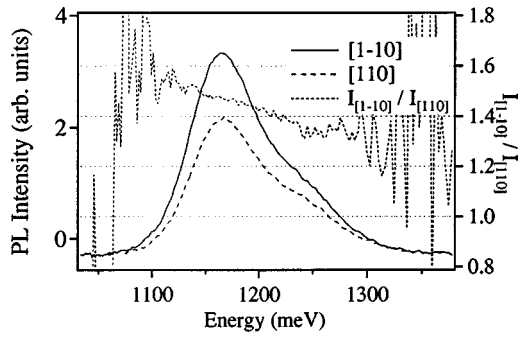

FIG. 10. Polarization-resolved PL spectra for InAs QD's grown at 500 °C and capped at 450 °C. The polarization ratio between the [1-10] and [110] directions for the ground transition at 1175 meV is 1.45.

QD's are smaller than in the samples whose spectra are depicted in Fig. 8. While further study is clearly needed to disentangle the effect of growth and capping procedures on dot size, shape, and degree of intermixing (these parameters are experimentally confounded), it seems likely that differences in growth conditions may explain the different polarization ratios $I_{[1\bar{1}0]}/I_{[110]}$ for the ground PL transition previously reported by different investigators, which range from 2 (Ref. 28) to 1.37,[49] to 1.2 (this work).

Another analysis of the optical polarization anisotropy was made by Wang *et al.*, who used the empirical pseudopotential method to model the electronic structure of self-organized InAs/GaAs QD's, assuming a square-based pyramidal shape with {101} facets.[45] This paper showed an atomic-level asymmetry of the carrier wave functions, which gives rise to an in-plane optical polarization anisotropy. The asymmetry originates from the atomistic structure of the QD/barrier interface, and is distinct in origin from both the strain asymmetry described in Sec. III of this paper and shape effects. By neglecting this atomistic effect in our calculation, which utilizes a continuum description of the interface, some error is incurred. However, the atomistic asymmetry should be significantly more sensitive to interface disorder than the shape effect. As discussed in Ref. 50, the QD/barrier interface becomes disordered in the process of capping, an effect not included in the pseudopotential calculation of Wang *et al.* However, the shape contribution to the anisotropy is relatively insensitive to the precise interface structure. For example, rounding of the QD facets has little effect on the polarization anisotropy. To illustrate this point, in Fig. 12 we compare the calculated polarization-dependent OME's for a dot bounded by {136} facets to a dot with an elongated lens-shape having a similar aspect ratio. The electronic structure and optical polarization anisotropy are quite similar for these two model structures as expected.

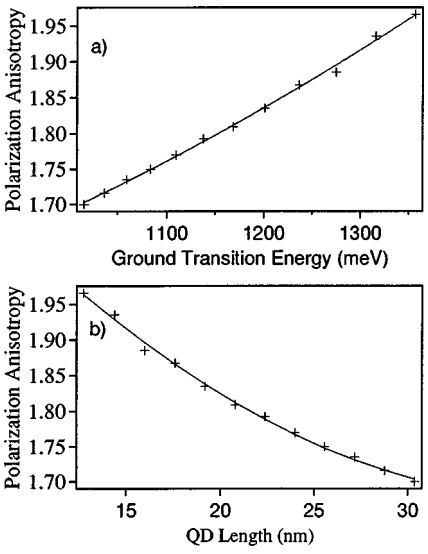

FIG. 11. Size dependence of polarization anisotropy. The calculated ratio $I_{[1\bar{1}0]}/I_{[110]}$ for the {136} structure is plotted versus ground transition energy in panel (a) and versus QD length in panel (b).

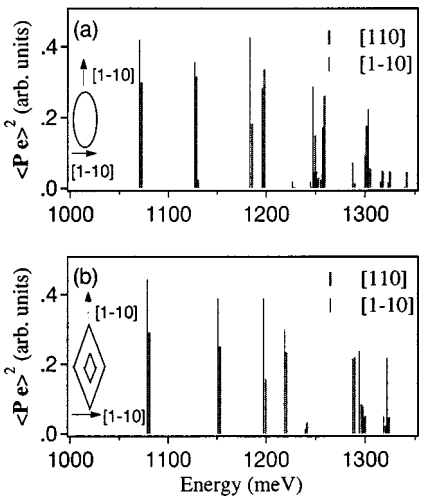

FIG. 12. Polarization-dependent optical matrix elements calculated for elongated lens-shaped dot compared to faceted dot. (a) Elongated len-shaped dot. The upper boundary of the dot obeys the equation $(x/r_a)^2+(y/r_b)^2+(z/r_c)^2=1$ where $r_a=68$ nm, $r_b=34$ nm, and $r_c=34$ nm, and is cut so that the length: width:height ratio of the dot is 18:9:1 versus 16:8:1 for the truncated {136} dot shown in panel (b).

VI. CONCLUSIONS

Evidence from RHEED, AFM, and high resolution cross-sectional TEM studies indicates that prior to capping, self-organized InAs QD's grown by MBE on GaAs [001] substrate are nanopyramids elongated along the $[1\bar{1}0]$ direction, with bounding facets corresponding to four {136} facets. This shape is quite different from the high symmetry shapes assumed in previous electronic structure calculations for this system. We have studied the effect of the geometrical asymmetry of the {136} structure on the electronic structure and optical polarization properties. Using an eight-band $\vec{k}\cdot\vec{p}$ electronic structure method including atomistically determined strain, our calculations on the {136} structure show good agreement with polarization-resolved PL experiments, particularly when the top of the {136} structure is truncated with (001) plane. Specifically, the model predicts an overall polarization anisotropy oriented towards $[1\bar{1}0]$ and a spectral shift of the second major excited state transition with polarization which are both observed experimentally. The model also predicts that the polarization anisotropy should

decrease with increasing dot size. Other findings are that strain and quantum confinement effects compensate to a degree in self-organized dots to produce an approximate linear scaling of QD eigenenergies with size rather than the quadratic scaling expected in simple effective mass models.

Some discrepancies exist between the electronic structure model and the experimental PL spectra, for example, the polarization anisotropy calculated for the unmodified {136} structure is larger than the observed anisotropy. It is likely that these quantitative discrepancies are a consequence of shape changes or intermixing effects during GaAs overgrowth not accounted for in the model. To fully understand the electronic structure of QD's, a more thorough study of the effect of capping on the QD shape, composition, and interface structure is clearly needed. Further detailed comparison between the experiment and theory will also require improvements in spectral resolution such as application of single-dot spectroscopy methods to overcome inhomogeneous broadening effects. These issues will be the focus of future experimental and theoretical investigations.

ACKNOWLEDGMENTS

This material is based upon work supported by the Army Research Office under Grant No. DAAH 04-96-1-0091. The authors would like to thank Craig Pryor and Wolfram Arnold for their technical help and discussion. R. Leon and C. Lobo are thanked for providing $In_xGa_{1-x}As$ quantum well samples used in this study.

[1] D. Leonard, M. Krishnamurthy, C.M. Reaves, S.P. Denbaars, and P.M. Petroff, Appl. Phys. Lett. **63**, 3203 (1993).
[2] G. Wang, S. Fafard, D. Leonard, J.E. Bowers, J.L. Merz, and P.M. Petroff, Appl. Phys. Lett. **64**, 2815 (1994).
[3] J.-Y. Marzin, J.-M. Gerard, A. Izrael, D. Barrier, and G. Bastard, Phys. Rev. Lett. **73**, 716 (1994).
[4] R. Leon, P.M. Petroff, D. Leonard, and S. Fafard, Science **267**, 1966 (1995).
[5] M. Grundmann, J. Christen, N.N. Ledentsov, J. Bohrer, D. Bimberg, S.S. Ruvimov, P. Werner, U. Richter, U. Gosele, J. Heydenreich, V. M. Ustinov, A. Yu. Egorov, A.E. Zhukov, P.S. Kop'ev, and Zh.I. Alferov, Phys. Rev. Lett. **74**, 4043 (1995).
[6] S. Fafard, R. Leon, D. Leonard, J.L. Merz, and P.M. Petroff, Phys. Rev. B **52**, 5752 (1995).
[7] M. Grundmann, N.N. Ledentsov, O. Stier, D. Bimberg, V. M. Ustinov, P.S. Kop'ev, and Zh.I. Alferov, Appl. Phys. Lett. **68**, 979 (1996).
[8] R. Heitz, M. Grundmann, N.N. Ledentsov, L. Eckey, M. Veit, D. Bimberg, V.M. Ustinov, A. Yu. Egorov, A.E. Zhukov, P.S. Kop'ev, and Zh.I. Alferov, Appl. Phys. Lett. **68**, 361 (1996).
[9] K.H. Schmidt, G. Medeiros-Ribeiro, M. Oestreich, P.M. Petroff, and G.H. Dohler, Phys. Rev. B **54**, 11 346 (1996).
[10] Weidong Yang, Hao Lee, Roger R. Lowe-Webb, and Peter C. Sercel, Phys. Rev. B **56**, 13314 (1997).
[11] H. Drexler, D. Leonard, W. Hansen, J.P. Kotthaus, and P.M. Petroff, Phys. Rev. Lett. **73**, 2252 (1994).
[12] G. Madeiros-Ribeiro, D. Leonard, and P.M. Petroff, Appl. Phys. Lett. **66**, 1767 (1995).
[13] D. Leonard, K. Pond, and P.M. Petroff, Phys. Rev. B **50**, 11 687 (1994).
[14] J.M. Moisson, F. Houzay, F. Barthe, L. Leprince, E. Andre, and O. Vatel, Appl. Phys. Lett. **64**, 196 (1994).
[15] Hao Lee, Weidong Yang, and Peter C. Sercel, Phys. Rev. B **55**, 9757 (1997).
[16] J.-Y. Marzin and G. Bastard, Solid State Commun. **92**, 437 (1994).
[17] A. Wojs, P. Hawrylak, S. Fafard, and L. Jacak, Phys. Rev. B **54**, 5604 (1996).
[18] S. Ruvimov and K. Scheerschmidt, Phys. Status Solidi A **150**, 471 (1995).
[19] M. Grundmann, O. Stier, and D. Bimberg, Phys. Rev. B **52**, 11 969 (1995).
[20] M.A. Cusack, P.R. Bridden, and M. Jaros, Phys. Rev. B **54**, R2300 (1996).
[21] Hongtao Jiang and Jasprit Singh, Phys. Rev. B **56**, 4696 (1997).
[22] Craig Pryor, Phys. Rev. B **57**, 7190 (1998).
[23] X. Z. Liao, J. Zou, X. F. Duan, D. J. H. Cockayne, R. Leon, and C. Lobo, Phys. Rev. B **58**, R4235 (1998).
[24] H. Lee Lowe-Webb, W. Yang, and P.C. Sercel, Appl. Phys. Lett. **72**, 812 (1998).
[25] H. Saito, K. Nishi, and S. Sugou, Appl. Phys. Lett. **74**, 1224 (1999).
[26] H. Lee, W. Yang, P.C. Sercel, and A. G. Norman, J. Electron. Mater. **28**, 481 (1999).
[27] S. Yoon, Y. Moon, T.-W. Lee, H. Hwang, E. Yoon, and Y. D. Kim, Thin Solid Films **357**, 81 (1999).
[28] Y. Nabetani, T. Ishikawa, S. Noda, and A. Sasaki, J. Appl. Phys. **76**, 3347 (1994).
[29] R.P. Mirin J.P. Ibbetson, K. Nishi, A.C. Gossard, and J.E. Bowers, Appl. Phys. Lett. **67**, 3795 (1995).
[30] G.E. Pikus and G.L. Bir, Fiz. Tverd. Tela (Leningrad) **1**, 1642 (1959) [Sov. Phys. Solid State **1**, 1502 (1960)].
[31] P.N. Keating, Phys. Rev. **145**, 637 (1966).
[32] R.M. Martin, Phys. Rev. B **1**, 4005 (1969).
[33] J.E. Bernard and A. Zunger, Appl. Phys. Lett. **65**, 165 (1994).
[34] A. Silverman, A. Zunger, R. Kalish, and J. Adler, Phys. Rev. B **51**, 10 795 (1995).
[35] F. Glas, J. Appl. Phys. **66**, 1667 (1989).
[36] C. Pryor, J. Kim, L.W. Wang, A.J. Williamson, and A. Zunger, J. Appl. Phys. **83**, 2548 (1998).
[37] C.G. Van der Walle, Phys. Rev. B **39**, 1871 (1989).
[38] J.M. Luttinger and W. Kohn, Phys. Rev. **97**, 869 (1955).
[39] J.M. Luttinger, Phys. Rev. **102**, 1030 (1956).
[40] C.R. Pidgeon and R.N. Brown, Phys. Rev. **146**, 575 (1966).
[41] T.B. Bahder, Phys. Rev. B **41**, 11 992 (1990).
[42] *Semiconductors: Physics of Group IV Elements and III-V Compounds*, edited by O. Madelung, M. Schulz, and H. Weiss, Landolt-Börnstein, New Series, Group III, Vol. 17, Pt. a (Springer-Verlag, Berlin, 1982).
[43] R.A. Morrow and K.R. Brownstein, Phys. Rev. B **30**, 678 (1984).
[44] R. Lehoucq, K. Maschhoff, D. Sorensen, and C. Yang, http://www.caam.rice.edu /~kristen/parpack_home.html; (unpublished).

[45] Lin-Wang Wang, Jeongnim Kim, and Alex Zunger, Phys. Rev. B **59**, 5678 (1999).
[46] Jeongnim Kim, Lin-Wang Wang, and Alex Zunger, Phys. Rev. B **57**, R9408 (1998).
[47] J.M. Garcia, G. Medeiros-Ribeiro, K. Schmidt, T. Ngo, J.L. Feng, A. Lorke, J. Kotthaus, and P.M. Petroff, Appl. Phys. Lett. **71**, 2014 (1997).
[48] W. Wu, J.R. Tucker, G.S. Solomon, and J.S. Harris, Jr., Appl. Phys. Lett. **71**, 1083 (1997).
[49] H. Saito, K. Nishi, S. Sugou, and Y. Sugimoto, Appl. Phys. Lett. **71**, 590 (1997).
[50] P.B. Joyce, T.J. Krzyzewski, G.R. Bell, B.A. Joyce, and T.S. Jones, Phys. Rev. B **58**, R15 981 (1998).